Desorption kinetics of O and CO from Graphitic Carbon Surfaces

Krishnan Swaminathan-Gopalan,*
Science and Technology Corporation at NASA Ames Research Center, Moffett Field, CA, 94035, USA.

and Kelly A. Stephani†
Department of Mechanical Science and Engineering, University of Illinois at Urbana-Champaign, Urbana, IL, 61801, USA.

The desorption of O/CO from graphitic carbon surfaces is investigated using a one-dimensional model describing the adsorbate interactions with the surface phonon bath. The kinetics of desorption are described through the solution of a master equation for the time-dependent population of the adsorbate in an oscillator state, which is modified through thermal fluctuations at the surface. The interaction of the adsorbate with the surface phonons is explicitly captured by using the computed phonon density Of states (PDOS) of the surface. The coupling of the adsorbate with the phonon bath results in the transition of the adsorbate up and down a vibrational ladder. The adsorbate-surface interaction is represented in the model using a Morse potential, which allows for the desorption process to be directly modeled as a transition from bound to free (continuum) state. The PDOS is a property of the material and the lattice; and is highly sensitive to the presence of defects. The effect of etch pits along with random surface defects on the PDOS is considered in the present work. The presence of defects causes a redshift and broadening of the PDOS, which in turn changes the phonon frequency modes available for adsorbate coupling at the surface. Using the realistic PDOS distributions, the phonon-induced desorption (PID) model was used to compute the transition and desorption rates for both pristine and defective systems. Mathissen's rule is used to compute the phonon relaxation time for pristine and defective systems based on the phonon scattering times for each of the different scattering processes. First, the desorption rates of the pristine system is fitted against the experimental values to obtain the Morse potential parameters for each of the observed adatoms. These Morse potential parameters are used along with the defective PDOS and phonon relaxation time to compute the desorption rates for the defective system. The defective system rates (both transition and desorption) were consistently lower in comparison with the pristine system. The difference between the transition rates is more significant at lower initial states due to higher energy spacing between the levels. In the case of the desorption rates, the difference between the defective and pristine system is more significant at higher temperatures. The desorption rates for each of the system shows an order of magnitude decrease with the strongly bound systems exhibiting the greatest reduction in the desorption rates.

Nomenclature

b	creation operator
$b^\dagger$	annihilation operator
D	Diameter
E	Energy
g	Phonon density of states (PDOS)
H	Hamiltonian, Height
$\hbar$	Planck's constant
P	Probability
Ph	Phonons
k	Rate constant
t	Time
V	Potential
v	Velocity

*Research Scientist, Member AIAA.
†Assistant Professor, Associate Fellow AIAA.

ω	Frequency
θ	Surface coverage
ρ	Density matrix, Density of defects
τ	Characteristic time
MD	Molecular Dynamics
$PDOS$	Phonon density of states
PID	Phonon induced desorption
TPS	Thermal protection system
$conj$	conjugate
des	Desorption
$over$	over-coordination
pen	penalty
$tors$	torsion
$under$	under-coordination
val	valence
$vdWaals$	van der Waals

I. Introduction

The density and energy of phonons present at the surface is described using the phonon density of states (PDOS). The PDOS is a fundamental property of the material and the lattice, which characterizes the distribution of allowed vibrational modes. The PDOS can provide information regarding thermal, optical, mechanical, electrical, chemical, and transport properties of the material. While the PDOS is primarily a function of the local atomic structure, it is also sensitive to atomic-level stresses and the microstructure. The presence of adsorbates and defects on the surface are known to cause deviations to the PDOS from the corresponding bulk structure. Thus, it is natural to expect that even small concentrations of defects in graphitic carbon may lead to specific shifts, broadenings and additional characteristic singularities in the phonon densities of states and thus change the material specific heat and transport properties. Such effects in carbon materials used as Thermal Protection System (TPS) are very significant because of the continual change in the lattice of the material owing to the reactive interaction and erosion due to ablation.

Changes in the phonon density of states not only affect the material thermo-physical properties, it also affects the adsorption and reaction rates and thereby the ablation and recession rates. Although the effects of point defects caused due to irradiation on graphite has been examined previously in the literature,[1,2,3,4,5] the main type of defect encountered during ablation is etch pits occurring as a result of oxidation reaction due to atomic oxygen. The effect of such etch pits individually and in the presence of point defects (perhaps introduced by fabrication/processing) needs to be studied.

Many commonly used TPS materials consist of a carbon-based substrate such as FiberForm®[6] and carbon weaves.[7] The primary source of carbon ablation at lower temperatures is through oxidation, specifically due to dissociated atomic oxygen.[8] Recent studies have elucidated that the oxidation products CO and CO_2 are formed as a result of thermal processes on the surface.[9,10,11,12] Desorption of thermal products from the substrate occur through the interaction with the phonon bath on the surface. Several finite-rate reaction models exist for the air-carbon system,[8,13,14,15,12] developed using results from numerous experimental studies.[9,16,17,18,19,20,21] However, all of these models characterize the rate of desorption only as a function of temperature. The effect on the desorption rate due to variations in the surface phonons, which is a function of the surface structure and configuration, needs to be characterized for these systems. A mesoscale description of the surface energetics which participate in, and promote the desorption of surface adsorbates and oxidation products is currently lacking.

In this study, a rigorous theoretical model is used to describe the desorption of adsorbed atoms/molecules due to interaction with the surface phonons.[22] The adsorbate-surface interaction (oscillator) is coupled with the phonon bath leading to excitations and de-excitations along the vibrational 'ladder'. This process can be described as a random walk using the Markoffian approximation and first order master equation is solved for the probability in a given state. This random walk continues until the interaction energy becomes sufficient to break the adsorbate-surface bond leading to desorption. Traditionally, simple harmonic oscillators (SHO) are used to describe the vibrational bond.[23]

However, within the harmonic approximation, the bond breaking is not inherently captured and has to be imposed, typically as a vibrational threshold beyond which desorption is assumed. In addition, the energy spacing between the oscillator levels is constant within the SHO approximation, which becomes particularly poor at the higher energy levels. Furthermore, the SHO allows only mono-quantum jumps, which again breaks down at higher energy levels. The Morse potential provides a much better approximation to the adsorbate surface bond with decreasing energy gaps at higher levels, finite probability of multi-quantum transitions and a clear threshold between the free and bound states. Thus, the Morse potential is employed within this framework to describe the adsorbate-surface interaction potential.[22]

The transition matrix describing the probability of transition between the oscillator energy levels accounts for the PDOS present at the surface. The coupling of the oscillator jump with each of the phonon modes is summed to give the final transition rate. Thus, introducing a realistic PDOS within the calculation of the transition matrix ensures the accurate description of the transition rates and thereby the desorption rate. The time between successive transitions (jumps) of a particular surface-adsorbate oscillator within the vibrational ladder is known to be much higher than the characteristic vibrations of the adsorbate and surface atoms.[24] This fact allows the treatment of these transition processes as rare events and use Markoffian random walks to analyze them. The desorption process is treated as first order and a Master equation is used to derive the final rate constant.[22]

This paper is organized as follows. The theoretical framework describing the phonon-induced desorption process is presented in Section II. The computation of the PDOS for the pristine and the defective systems using MD, that is incorporated into this framework, is described in Section III. Section IV. describes the process of computing the transition and desorption rates for the different systems of interest. The results of this study are discussed in Section V., and the transition rates and the desorption rates of the pristine and defective systems are compared and analyzed. Finally the conclusions and summary are presented in Section VI.

II. Phonon-induced Desorption Model

In order to describe the desorption of adsorbed atoms/molecules from the surface due to the interaction with the phonon bath, the theory by Efrima *et al.*[22] is used. This theory begins by describing the Hamiltonian of the system which consists of three parts: lattice (l), particle (p) and interaction (I).[22]

$$H = H_l + H_p + H_I \tag{1a}$$

$$H_l = \hbar \sum_{\lambda} \omega_\lambda b_\lambda^\dagger b_\lambda \tag{1b}$$

$$H_p = K_p + \langle V(\boldsymbol{Q}; z) \rangle \tag{1c}$$

$$H_I = V(\boldsymbol{Q}; z) - \langle V(\boldsymbol{Q}; z) \rangle \tag{1d}$$

The lattice Hamiltonian is described over the phonons (λ) in the system. ω is the phonon frequency while b and $b^\dagger$ are the corresponding creation and annihilation operators. K_p is the kinetic energy of the particle, $V(\boldsymbol{Q}; z)$ is the interaction potential between the adsorbate and the surface atom, and $\langle V(\boldsymbol{Q}; z) \rangle$ is the thermal average of the lattice-particle interaction over an equilibrium phonon distribution. $\boldsymbol{Q}$ is 3N dimensional and denotes the position of the N lattice atoms and z is the position of the adsorbed particle. $H_l + H_p$ is the zero-order part of the Hamiltonian while H_I describes the fluctuations in the system. The reason for the addition of the average quantity $\langle V(\boldsymbol{Q}; z) \rangle$ is to ensure that the average of the interaction Hamiltonian is zero which avoids the buildup of secular terms in the subsequent derivation.[22] The adsorbate-surface interaction potential is described using a Morse potential:

$$V(\boldsymbol{Q}; z) = D \left\{ e^{-2\alpha(z - \boldsymbol{Q}_0 - \boldsymbol{u} - r_0)} - 2e^{-\alpha(z - \boldsymbol{Q}_0 - \boldsymbol{u} - r_0)} \right\} \tag{2}$$

where $\boldsymbol{Q}_0$ is the equilibrium lattice position and $\boldsymbol{u}$ is the displacement of the atoms. α and r_0 are the Morse potential parameters. The Morse potential is an excellent approximation for the adsorbate-particle interaction since it captures bond breaking (desorption), multi-quantum jumps, and decreasing energy spacing at higher energies. Thus, the definition of the bound states and free state within the model is straightforward and the ladder climbing pathway of desorption can be captured along with multi-quantum jumps (Fig. 1).

Now, the generalized master equation is presented, which describes the time evolution of the probability of the

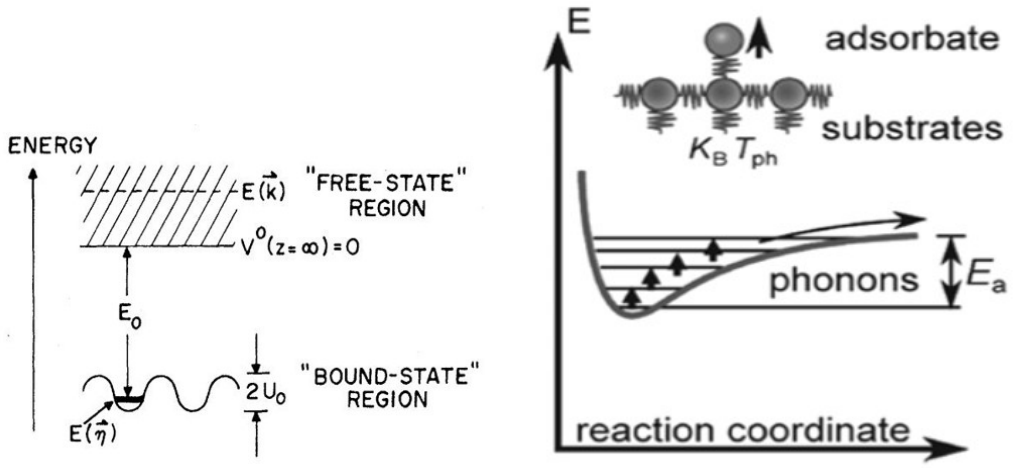

Figure 1: (a) Schematic showing the bound and free-state regions for an adsorbed particle. Reproduced with permission from Ref. 23. Copyright 1972 APS. (b) Ladder climbing model describing the pathway of desorption. Reproduced with permission from Ref. 25. Copyright 2010 Wiley.

adsorbates being present in a particular state $|n\rangle$ at time t:[22]

$$\frac{\partial P_n}{\partial t} = -\sum_m W_{n\to m} P_n(t) + \sum_m W_{m\to n} P_m(t) - \int W_{n\to\epsilon} P_n(t) d\epsilon \tag{3}$$

The first term on the right side of the equation describes the transitions from state n to all other states, while the second term represents all the transitions leading to the state n. The last term denotes the depletion from state n to the continuum state ϵ (desorption). Expressing $P_n(t)$ in terms of the reduced density matrix:[22]

$$P_n(t) = \langle n| \rho_r(t) |n\rangle . \tag{4}$$

Here, $\rho_r(t)$ is the reduced density matrix of the particle, defined as summation over all phonon states $|Ph\rangle$:

$$\rho_r(t) = \sum_{Ph} \langle Ph| \rho(t) |Ph\rangle . \tag{5}$$

The density matrix $\rho(t)$ of the lattice-particle system satisfies the Liouville equation:[22]

$$\frac{\partial \rho(t)}{\partial t} = -\frac{i}{\hbar} [H, \rho(t)] \tag{6}$$

Now substituting the Hamiltonian and $\rho(t)$ from the previous equations, the following expression is obtained for rate of probability:[22]

$$\begin{aligned} \frac{\partial P_n(t)}{\partial t} &= \int_0^t \sum_m K_{nm}(s) P_m(t-s) \\ K_{nm}(s) &= \frac{-2}{\hbar^2} Re \left\{ \sum_k e^{i\omega_{mk}} \langle (H_I(s))_{mk} (H_I)_{km} \rangle \delta_{nm} - e^{-i\omega_{nm} s} \langle (H_I(s))_{mn} (H_I)_{nm} \rangle \right\} \end{aligned} \tag{7}$$

Using a Markoffian approximation, the $K_{nm}(s)$ is assumed to decay on a time scale that is small enough such that the value of $P_n(t)$ is constant, resulting in[22]

$$\int_{-\infty}^t K_{nm}(s) P_m(t-s) ds \cong P_m(t) \int_{-\infty}^{\infty} K_{nm}(s) ds \cong \boldsymbol{W}_{nm} P_m(t) \tag{8}$$

with

$$\begin{aligned} \boldsymbol{W}_{nm} &= -\delta_{nm} \sum_k W_{m\to k} + W_{m\to n} \\ W_{n\to m} &= \frac{2}{\hbar^2} Re \left\{ \int_0^\infty \langle (H_I(s))_{mn} (H_I)_{nm} \rangle \, exp(+i\omega_{nm} s) \right\} \end{aligned} \tag{9}$$

Assuming a first order master equation, $P(t)$ can be expressed as:[22]

$$P(t) = e^{\boldsymbol{W}t} P(0) \tag{10}$$

Using this, the average time between two successive desorption events can be calculated as:[22]

$$\langle \tau \rangle = \sum_n \int_0^\infty P_n(t) dt = \sum_n \left(\boldsymbol{W}^{-1} P(0) \right)_n \tag{11}$$

The desorption rate is given by the inverse of the average time.

$$k_{des} = \langle \tau \rangle^{-1} \tag{12}$$

Thus, all that is required now to calculate the desorption rate constants is the phonon density of states and the transition rates. There are two types of transition present in the system: bound to bound, and bound to continuum. The bound to bound transition rates can be derived as:[26]

$$\begin{aligned} W_{n\to m} =& \frac{2D^2}{\hbar^2} Re \int_0^\infty dt \, exp(i\omega_{nm} t) \\ & \Big[\left(B_{nm}^{(2)} \right)^2 exp\left(4\alpha^2 \left\langle u^2 \right\rangle\right) \left\{ exp\left(4\alpha^2 \left\langle u(t)u(0) \right\rangle\right) - 1 \right\} \\ & + 4 \left(B_{nm}^{(1)} \right)^2 exp\left(\alpha^2 \left\langle u^2 \right\rangle\right) \left\{ exp\left(\alpha^2 \left\langle u(t)u(0) \right\rangle\right) - 1 \right\} \\ & - 4 \left(B_{nm}^{(1)} \right) \left(B_{nm}^{(2)} \right) exp\left(2.5\alpha^2 \left\langle u^2 \right\rangle\right) \left\{ exp\left(2\alpha^2 \left\langle u(t)u(0) \right\rangle\right) - 1 \right\} \Big] \end{aligned} \tag{13}$$

The term $B_{nm}^{(j)}$ is the bound to bound matrix elements, for which a general expression can be obtained as:[22]

$$\begin{aligned} B_{nm}^{(j)} =& \frac{1}{2k} \left[\frac{\tilde{n}(2k - \tilde{n} - 1) - \bar{n}(2k - \bar{n} - 1) + 2k}{2k} \right]^{j-1} \\ & \tilde{n}! \, \Gamma(2k - \tilde{n}) \left[\frac{(2k - 2\tilde{n} - 1)(2k - 2\bar{n} - 1)}{\tilde{n}! \Gamma(2k - \tilde{n}) \bar{n}! \Gamma(2k - \bar{n})} \right]^{1/2} \end{aligned} \tag{14}$$

Here $\langle u(t)u(0) \rangle$ is the correlation function of surface atom displacement given by

$$\langle u(t)u(0) \rangle = \frac{\hbar}{2M} \int_0^\infty d\omega \rho(\omega) \left| \zeta(\omega) \right|^2 \left\{ n(\omega) e^{-i\omega t} + (n(\omega) + 1) \, e^{i\omega t} \right\} \frac{f(\Delta)}{\omega} \tag{15}$$

Here M is the mass of a lattice atom, while the quantities $\rho(\omega)$, $\zeta(\omega)$, and $n(\omega)$ are the phonon density of states, polarization, and population, respectively. The form of function $f(\Delta)$ appearing in the above equation determined by the choice of phonon relaxation model. The Lorentzian model of phonon broadening defines

$$f(\Delta) = exp(-\Delta |t|) \tag{16}$$

while the Gaussian model employs

$$f(\Delta) = exp(-\Delta^2 t^2 / 2) \tag{17}$$

The bound to continuum transition states can be defined in a similar manner:[22]

$$\begin{aligned} W_n =& \frac{2D^2}{\hbar^2} Re \int_0^\infty dt\, exp(i\omega_{n\epsilon} t) \\ & \Big[\Big(a^{(2)}(t) \Big)\, exp\left(4\alpha^2 \left\langle u^2 \right\rangle\right) \left\{ exp\left(4\alpha^2 \left\langle u(t)u(0) \right\rangle\right) - 1 \right\} \\ & + \Big(a^{(1)}(t) \Big)\, exp\left(\alpha^2 \left\langle u^2 \right\rangle\right) \left\{ exp\left(\alpha^2 \left\langle u(t)u(0) \right\rangle\right) - 1 \right\} \\ & - 4\,(c(t))\, \Big(B^{(2)}_{nm} \Big)\, exp\left(2.5\alpha^2 \left\langle u^2 \right\rangle\right) \left\{ exp\left(2\alpha^2 \left\langle u(t)u(0) \right\rangle\right) - 1 \right\} \Big] \end{aligned} \tag{18}$$

where the terms $a^{(j)}(t)$ and $c(t)$ are the bound to continuum matrix elements, for which a general expression can be obtained as:[22]

$$a^{(j)}(t) = \int_0^\infty d\epsilon\ exp(-i\omega_{n\epsilon} t)\ \left(B^{(j)}_{n\epsilon} \right)^2 \tag{19}$$

$$c(t) = \int_0^\infty d\epsilon\ exp(-i\omega_{n\epsilon} t)\ \left(B^{(1)}_{n\epsilon} B^{(2)}_{n\epsilon} \right) \tag{20}$$

III. PDOS of Defective Carbon Surfaces

The PDOS is calculated using the LAMMPS Molecular Dynamics (MD) software[27] through the determination of the velocity autocorrelation function.

$$g(\omega) = \int \frac{< v(t).v(0) >}{< v(0)^2 >} e^{i\omega t} dt \tag{21}$$

The ReaxFF inter-atomic potential is used to describe the C-C, C-O, and C-N interactions. ReaxFF potential is an empirical potential with a general form for various types of forces.[28]

$$E_{system} = E_{bond} + E_{over} + E_{under} + E_{val} + E_{pen} + E_{tors} + E_{conj} + E_{vdWaals} + E_{Coulomb}. \tag{22}$$

The various parameters within this form are parameterized against an extensive quantum chemical database. The value of the parameters used in this study are taken from Shin *et al*.[29] The C-C bond parameters used in this work were recently re-parameterized to better capture the properties of the solid carbon phase.[30] The ReaxFF potential and the corresponding set of parameters were chosen because they can capture both short and long range bonds within solid carbon[31] as well as the reactive interaction between the carbon and adsorbate atoms.[32]

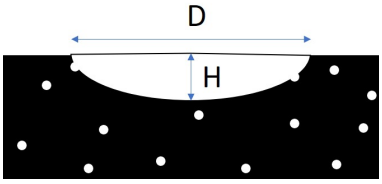

Figure 2: Schematic illustration of the side view of the lattice with an etch pit and random surface roughness.

The effect of the presence of etch pits along with random surface roughness on the PDOS is studied. The etch pits are formed due to oxidation processes and are ellipsoidal in shape.[33] These etch pits are characterized based on the depth (or height H) and diameter of the ellipsoid as shown in Fig. 2. The diameter of these etch pits are usually much higher than the height (or depth). This is because the oxidation along the lateral direction is much faster than along the normal direction.[33] These etch pits are directly obtained in MD by removing the atoms within the ellipsoidal region of pristine graphite lattice. The values of D and H are chosen to emulate the D:H ratio found in the experiments.

The random surface defects are present on engineering materials due to a wide variety of reasons such as manufacturing defects, irradiation damage, etc. Within the MD simulations, these regions are created on the graphite carbon

by irradiation with low energy ions. The surface defects are characterized based on the depth (height H) of the defective region and the areal density (number of defects per unit area ρ) as shown in Fig. 2. Pristine graphite lattice is bombarded with ions of different energies to obtain the desired defect configurations of different depths and densities.

Fig. 3 shows the effect of variation in the diameter and height of the etch pit. The surface roughness was kept constant at H = 18 Å and ρ = 18 Å^{-2}. Additional modes at very low energies are also observed for the defective surfaces. In general, the presence of surface roughness systematically shifts the PDOS modes from higher to lower frequencies. However, additional densities at frequencies greater than the final peak of the pristine system are also observed. This is most likely a result of the close packing of defects at certain regions. The presence of etch pits tend to broaden the PDOS modes and more rounded peaks are observed. The PDOS is found to be insensitive to the geometry of the etch pits resulting in very similar density of states for a wide range of D and H values.

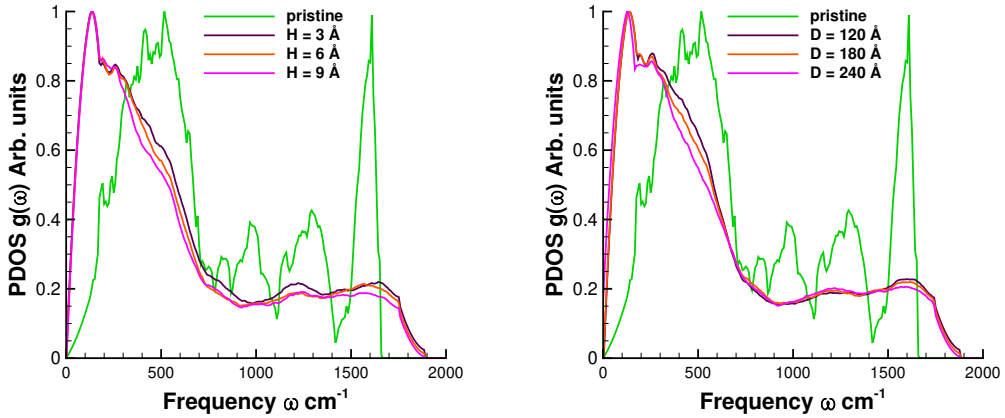

Figure 3: PDOS of carbon graphite surface with surface roughness and etch pit of (a) varying depths (heights) and (b) varying diameters.

IV. Calculations

A. Determination of input parameters

There are three main inputs to the theoretical model described in the previous section: surface-adatom (Morse) potential parameters, the phonon relaxation time, and the phonon density of states. The inter-atomic potential needs to describe the interaction between the adatom and the entire surface and not a single surface atom. Such potential parameters are not readily available in the literature. Further, these potential parameters are highly sensitive to the configuration of the adatom on the surface. Thus, these parameters are calibrated by fitting the desorption rates from this model to the values obtained from experimental data.[12]

The computation of the phonon relaxation time due to phonon interaction with various processes has been performed for both pristine and defective graphite.[34,35,36] Although the phonon relaxation time is a function of both temperature and frequency, a single value for each pristine and defective lattice is used. The phonon density of states as computed in the previous section is directly used for the calculations within the theoretical model. It is important to note that this PDOS is based on a graphitic carbon lattice (with an intra-layer atomic spacing of 1.42 Å and inter-layer spacing of 3.35 Å), while the desorption rates were developed for a vitreous carbon system. The phonon density of states for the vitreous carbon is expected to be different from that of the graphitic surface. Thus, the calibration of the interatomic Morse potential parameters are required in order to match the experimental results with the PID model.

The Morse potential parameters for each of the three different adatom configuration of O{a}, CO{a}, and CO{b} are calibrated by fitting the corresponding experimental desorption rates constants with those obtained from the theoretical model. For this calibration, the phonon density of states and phonon relaxation times corresponding to the pristine carbon system are employed. This is justified from the fact that the SEM images of the carbon sample obtained pre and post experiments showed negligible differences. Thus, it is postulated that due to the low input flux of oxygen, the carbon sample remains (nearly) topographically pristine throughout the experiments.

B. Desorption rates for defective systems

The interaction potential is expected to be sensitive to the configuration of the adatom on the surface and less sensitive to the surface configuration around the adatom. Thus, in this study, the Morse potential parameters obtained using the pristine system are used to compute the rate constants for the defective system. The phonon density of states is directly obtained for the case of etch pits with random surface roughness with the defect configuration described in the previous section. Finally, the phonon relaxation time for the defective system is obtained using the parameters presented in Ref. 34. For the phonon relaxation, the Gaussian model is used instead of the Lorentzian following the recommendation of Hood *et al.*[26] They observed that the transition rates predicted by the Lorentzian model were anomalously large, which is an artifact of the slower decay. Thus, the Gaussian model was used in all calculations.

V. Results and Discussion

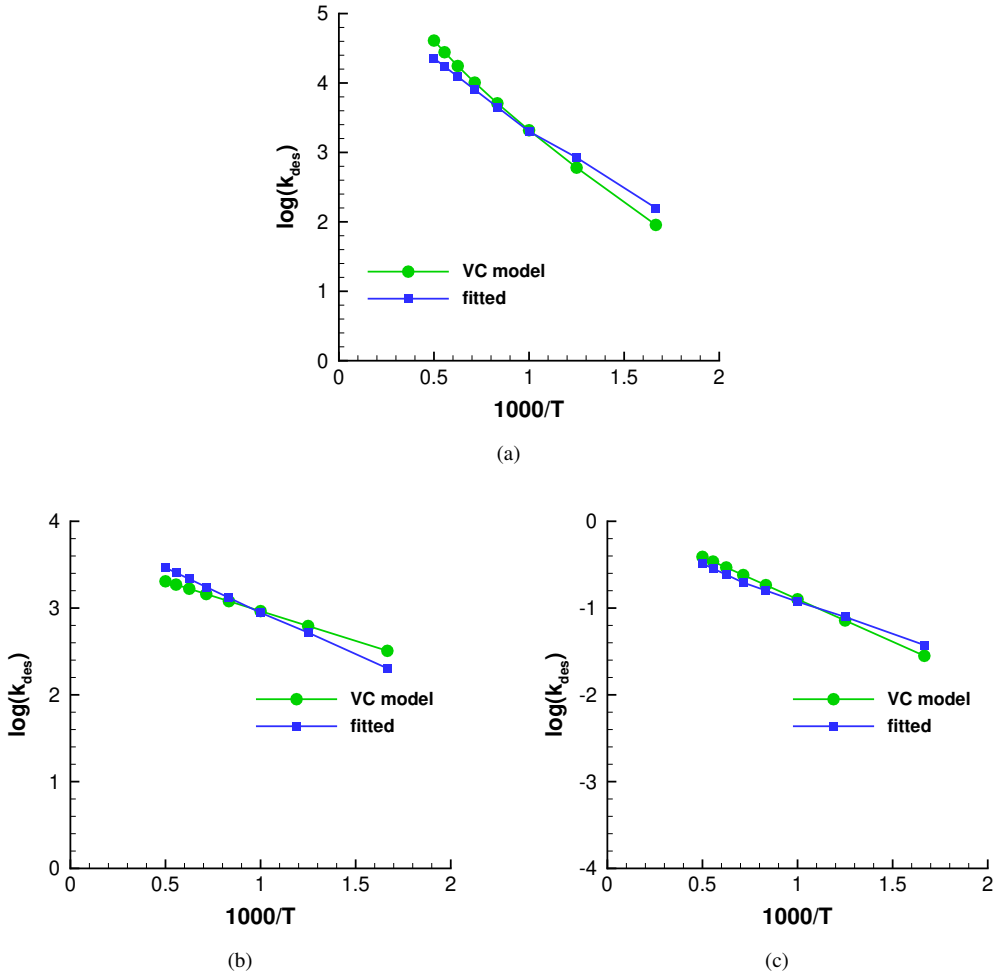

Figure 4: Rate constants for (a) O{a}, (b) CO{a}, and (c) CO{b} adatom systems from experiments[12] and theoretical model with a pristine carbon lattice.

The process of obtaining the Morse potential parameters by fitting the desorption rate constants of the pristine system is performed using least square method over the temperature range of interest. Fig. 4 presents the experimental and fitted rate constants for all the three adatom systems: O{a}, CO{a}, and CO{b}. The logarithm of the desorption rate constants are plotted against the inverse temperature. The experimental rate constants follow an Arrhenius form and thus forms a straight line. It is observed that the model predicts rate constants that deviate from the Arrhenius

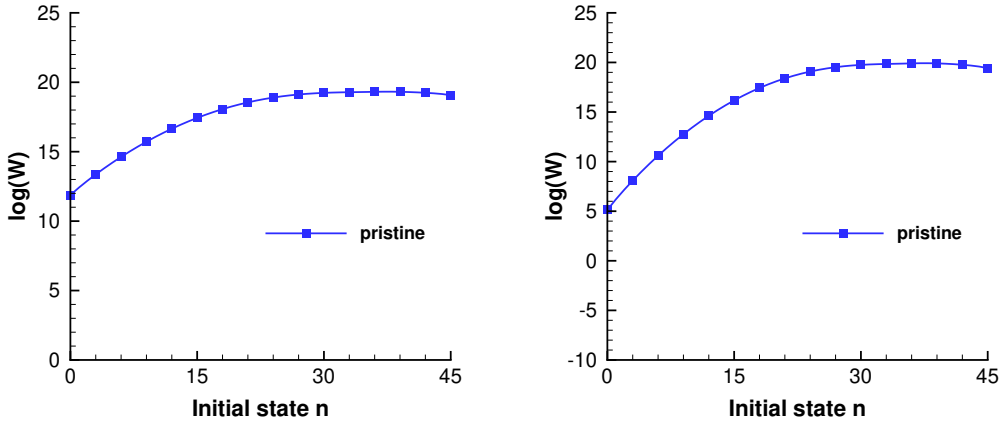

Figure 5: (a) Bound to bound and (b) bound to continuum transition rates between nearest neighbor oscillator states $W_{n\to n+1}$ vs bound state for the CO{b} adatom system with a pristine carbon lattice.

form especially at the lower temperatures, which is consistent with the results of Hood *et al.*[26] Nevertheless, good agreement is observed between the model (fitted) and experimental rate constants. As mentioned previously, these calculations were performed assuming a pristine lattice system. The CO{b} adatom has the strongest bond with the surface and therefore the lowest desorption rate, while O{a} has the highest desorption rate.

In order to further analyze the system, the transition rates (logarithm) between nearest neighbor oscillator states $W_{n\to n+1}$ are plotted against the initial state n for the CO{b} system. Fig. 5 (a) shows the bound to bound transition rates, while the bound to continuum transition rates are presented in Fig. 5 (b). The transition rates initially increases with the bound state n as the energy spacing between the levels decrease. At higher energy states, the transition rates reach a peak and then plateaus.

Next, the transition and desorption rates are computed and analyzed for a defective system. The phonon density of states computed in the previous chapter along with the phonon relaxation time for the defective system is used. Fig. 6 presents the rate constants of the defective system for all the three adatom systems: O{a}, CO{a}, and CO{b}. The experimental and fitted rate constants are also plotted for comparison. As expected, the rate constants for the defective system are consistently lower compared to the pristine system for all the three adatom configurations. Due to the presence of the defects, the phonons are increasingly scattered,[37,38,39] thus reducing the energy transferred to the adatom leading to lower desorption rates. This effect is increasingly observed at higher temperatures, where there is a larger population of high energy phonons for the pristine system. The presence of defects scatters these phonons to lower energies, thus reducing the energy transfer to the adatom and lower desorption rates. The desorption rates for each of the system shows an order of magnitude decrease with the strongly bound CO{b} system exhibiting the greatest reduction in the desorption rates consistent with the above reasoning.

Finally, the transition rates with the pristine and defective carbon lattice for the CO{b} system is shown in Fig. 7. Both the bound-bound and bound-continuum transition rates between nearest neighbor oscillator states $W_{n\to n+1}$ are plotted against the initial state n. The transition rates for the defective system are consistently lower than the pristine system, consistent with the observations of the desorption rates. The disparity is more significant at lower initial states where the spacing between the energy levels is higher.

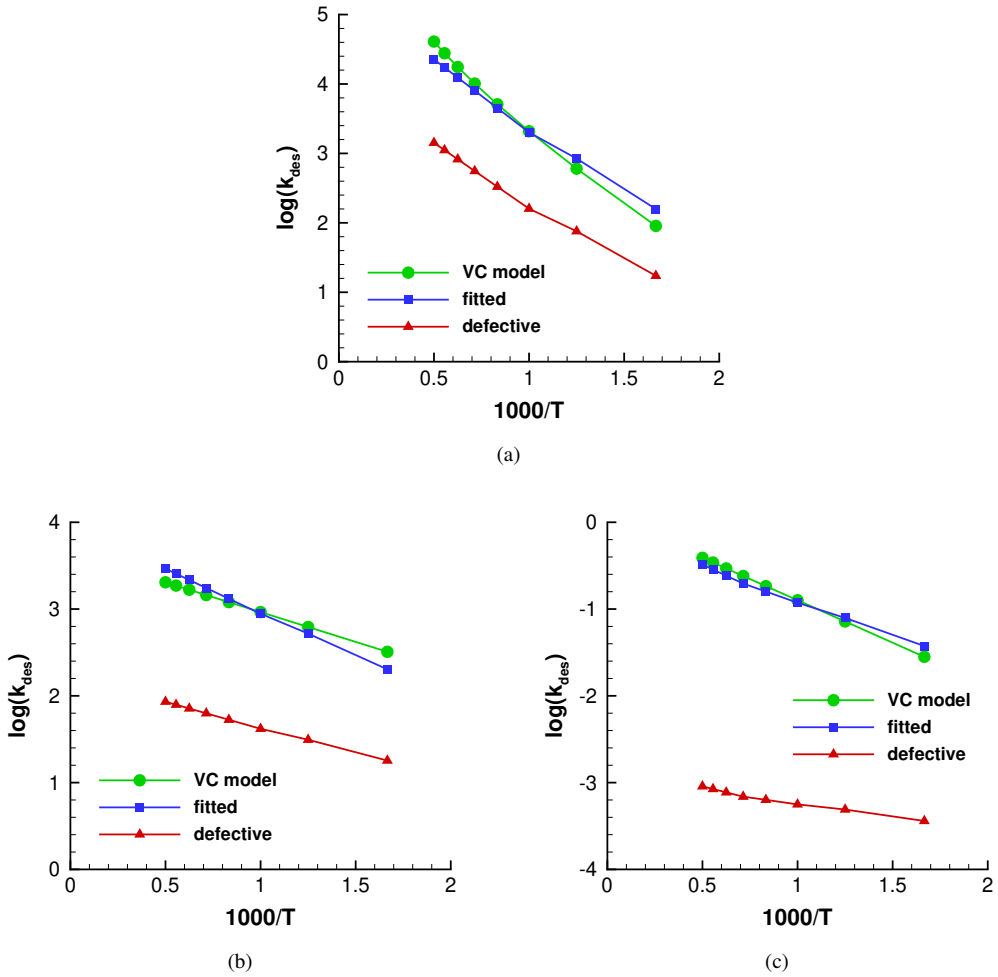

Figure 6: Rate constants for (a) O{a}, (b) CO{a}, and (c) CO{b} adatom systems from experiments[12] and theoretical model with a pristine and defective carbon lattice.

VI. Conclusions

A rigorous theoretical model based on the interaction of the adsorbed atoms/molecules with the phonon bath at the surface is used to describe the desorption process of the adsorbates. The interaction of the adsorbate with the surface phonons is explicitly captured by using the PDOS of the surface. The adsorbate-surface interaction is represented using a Morse potential, which allows for the desorption process (transition from bound to free state) to be directly modeled as the interaction energy reaches beyond a threshold level described by the potential. This model is one-dimensional and considers the interaction only along the surface normal direction. The coupling of the adsorbate with the phonon bath results in adsorbate-surface bond to jump within the interaction energy ladder. Both mono- and multi-quantum jumps are considered within this framework. The desorption process is treated as a Markoffian process and a first order Master equation is used to derive the final rate constant.

This model was used to compute the transition and desorption rates for both pristine and defective systems. The phonon density of states for both the pristine and defective systems are obtained directly from MD calculations. Mathissen's rule is used to compute the phonon relaxation time for pristine and defective systems based on the phonon scattering times for each of the different scattering processes. First, the desorption rates of the pristine system is fitted against the experimental values to obtain the Morse potential parameters for each of the three observed adatoms: O{a}, CO{a}, and CO{b}. These Morse potential parameters are used along with the defective PDOS and phonon relaxation time to compute the desorption rates for the defective system. The defective system rates (both transition and

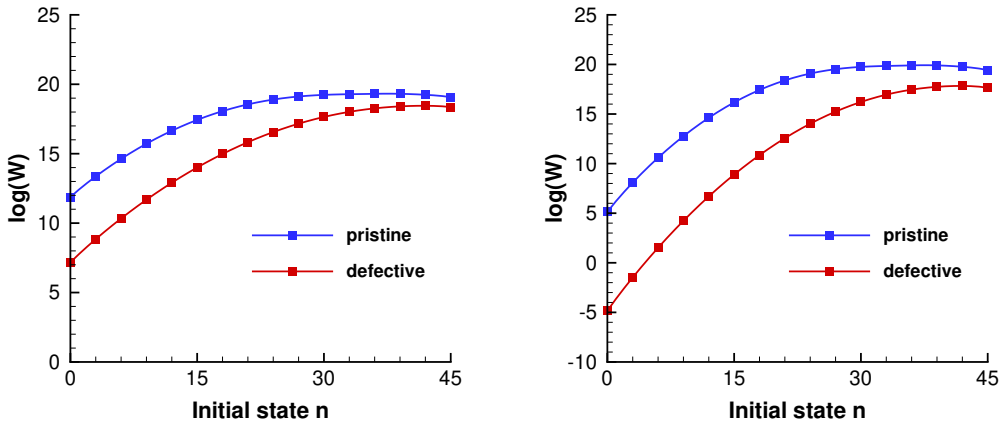

Figure 7: (a) Bound to bound and (b) bound to continuum transition rates between nearest neighbor oscillator states $W_{n\to n+1}$ vs bound state for the CO{b} adatom system for a pristine and defective carbon lattice.

desorption) were consistently lower in comparison with pristine system. This is a result of additional phonon scattering due to the presence of the defects leading to lower energy transfer to the adatom. The difference between the transition rates is more significant at lower initial states due to higher energy spacing between the levels. In the case of the desorption rates, the difference between the defective and pristine system is more significant at higher temperatures. A larger population of higher energy phonons which is present in the pristine system at higher temperatures are scattered due to the defects resulting in the greater disparity. The desorption rates for each of the system shows an order of magnitude decrease with the strongly bound CO{b} system exhibiting the greatest reduction in the desorption rates.

Acknowledgements

This material is based upon work supported by the Air Force Office of Scientific Research under award number FA9550-17-1-0127.

References

[1]Kelly, B., "The effect of defects on the basal plane thermal conductivity of a graphite crystal," *Carbon*, Vol. 5, No. 3, 1967, pp. 247–260.

[2]Taylor, R., Kelly, B., and Gilchrist, K., "The thermal conductivity of fast neutron irradiated graphite," *Journal of Physics and Chemistry of Solids*, Vol. 30, No. 9, 1969, pp. 2251–2267.

[3]Nakamura, K. and Kitajima, M., "Ion-irradiation effects on the phonon correlation length of graphite studied by Raman spectroscopy," *Physical Review B*, Vol. 45, No. 1, 1992, pp. 78.

[4]Ishioka, K., Hase, M., Kitajima, M., and Ushida, K., "Ultrafast carrier and phonon dynamics in ion-irradiated graphite," *Applied Physics Letters*, Vol. 78, No. 25, 2001, pp. 3965–3967.

[5]Ferrari, A. C., "Raman spectroscopy of graphene and graphite: disorder, electron–phonon coupling, doping and nonadiabatic effects," *Solid state communications*, Vol. 143, No. 1-2, 2007, pp. 47–57.

[6]Christian, J. A., Wells, G., Lafleur, J. M., Verges, A., and Braun, R. D., "Extension of traditional entry, descent, and landing technologies for human Mars exploration," *Journal of spacecraft and rockets*, Vol. 45, No. 1, 2008, pp. 130–141.

[7]Cassell, A. M., Brivkalns, C. A., Bowles, J. V., Garcia, J. A., Kinney, D. J., Wercinski, P. F., Cianciolo, A. D., and Polsgrove, T. T., "Human Mars mission design study utilizing the adaptive deployable entry and placement technology," *Aerospace Conference, 2017 IEEE*, IEEE, 2017, pp. 1–16.

[8]Park, C., "Effects of atomic oxygen on graphite ablation," *AIAA Journal*, Vol. 14, No. 11, nov 1976, pp. 1640–1642.

[9]Murray, V. J., Marshall, B. C., Woodburn, P. J., and Minton, T. K., "Inelastic and Reactive Scattering Dynamics of Hyperthermal O and O2 on Hot Vitreous Carbon Surfaces," *Journal of Physical Chemistry C*, Vol. 119, No. 26, 2015, pp. 14780–14796.

[10]Poovathingal, S., Schwartzentruber, T. E., Murray, V. J., Minton, T. K., and Candler, G. V., "Finite-Rate Oxidation Model for Carbon Surfaces from Molecular Beam Experiments," *AIAA Journal*, Vol. 55, No. 5, 2017, pp. 1644–1658.

[11]Swaminathan Gopalan, K., Borner, A., Stephani, K. A., Poovathingal, S. J., Murray, V. J., Minton, T. K., and Mansour, N. N., "DSMC Analysis of Molecular Beam Experiments for Oxidation of Carbon Based Ablators," *55th AIAA Aerospace Sciences Meeting*, 2017, p. 1845.

[12]Swaminathan-Gopalan, K., Borner, A., Murray, V. J., Poovathingal, S., Minton, T. K., Mansour, N. N., and Stephani, K. A., "Development and validation of a finite-rate model for carbon oxidation by atomic oxygen," *Carbon*, Vol. 137, 2018, pp. 313–332.

[13]Zhluktov, S. V. and Abe, T., "Viscous Shock-Layer Simulation of Airflow past Ablating Blunt Body with Carbon Surface," *Journal of Thermophysics and Heat Transfer*, Vol. 13, No. 1, 1999, pp. 50–59.

[14]Alba, C. R., *A Nonequilibrium Finite-Rate Carbon Ablation Model for Radiating Earth Re-entry Flows*, Ph.D. thesis, Air Force Institute of Technology, Wright-Patterson Air Force Base, Ohio, 2015.

[15]Poovathingal, S., Schwartzentruber, T. E., Murray, V., Minton, T. K., and Candler, G. V., "Finite-rate oxidation model for carbon surfaces from molecular beam experiments," *46th AIAA Thermophysics Conference*, 2016, p. 3842.

[16]Allendorf, H. and Rosner, D., "Comparative studies of the attack of pyrolytic and isotropic graphite by atomic and molecular oxygen at high temperatures." *AIAA journal*, Vol. 6, No. 4, 1968, pp. 650–654.

[17]Allendorf, H. D. and Rosner, D. E., "Primary products in the attack of graphite by atomic oxygen and diatomic oxygen above 1100 K," *Carbon*, Vol. 7, No. 4, 1969, pp. 515–518.

[18]Rosner, D. and Allendorf, H., "High temperature oxidation of carbon by atomic oxygen," *Carbon*, Vol. 3, No. 2, 1965, pp. 153–156.

[19]Walls, J. and Strickland-Constable, R., "Oxidation of carbon between 1000–2400 C," *Carbon*, Vol. 1, No. 3, 1964, pp. 333IN23335–334338.

[20]Olander, D., Siekhaus, W., Jones, R., and Schwarz, J., "Reactions of modulated molecular beams with pyrolytic graphite. I. Oxidation of the basal plane," *The Journal of Chemical Physics*, Vol. 57, No. 1, 1972, pp. 408–420.

[21]Panerai, F., Martin, A., Mansour, N. N., Sepka, S. A., and Lachaud, J., "Flow-tube oxidation experiments on the carbon preform of a phenolic-impregnated carbon ablator," *Journal of Thermophysics and Heat Transfer*, Vol. 28, No. 2, 2014, pp. 181–190.

[22]Efrima, S., Jedrzejek, C., Freed, K. F., Hood, E., and Metiu, H., "A one-dimensional model for phonon-induced desorption," *The Journal of chemical physics*, Vol. 79, No. 5, 1983, pp. 2436–2453.

[23]Bendow, B. and Ying, S.-C., "Phonon-induced desorption of adatoms from crystal surfaces. I. Formal theory," *Physical Review B*, Vol. 7, No. 2, 1973, pp. 622.

[24]Gillespie, D. T., "A general method for numerically simulating the stochastic time evolution of coupled chemical reactions," *Journal of computational physics*, Vol. 22, No. 4, 1976, pp. 403–434.

[25]Funk, S., Bonn, M., Denzler, D., Hess, C., Wolf, M., and Ertl, G., "Desorption of CO from Ru (001) induced by near-infrared femtosecond laser pulses," *The Journal of Chemical Physics*, Vol. 112, No. 22, 2000, pp. 9888–9897.

[26]Hood, E., Jedrzejek, C., Freed, K. F., and Metiu, H., "A one-dimensional model for phonon-induced desorption. II. Numerical analysis of the desorption of noble gas atoms (argon, krypton, and xenon) from tungsten and carbon monoxide from copper," *The Journal of chemical physics*, Vol. 81, No. 7, 1984, pp. 3277–3293.

[27]Plimpton, S., "Fast parallel algorithms for short-range molecular dynamics," *Journal of computational physics*, Vol. 117, No. 1, 1995, pp. 1–19.

[28]Van Duin, A. C., Dasgupta, S., Lorant, F., and Goddard, W. A., "ReaxFF: a reactive force field for hydrocarbons," *The Journal of Physical Chemistry A*, Vol. 105, No. 41, 2001, pp. 9396–9409.

[29]Shin, Y. K., Gai, L., Raman, S., and Van Duin, A. C., "Development of a reaxff reactive force field for the pt–ni alloy catalyst," *The Journal of Physical Chemistry A*, Vol. 120, No. 41, 2016, pp. 8044–8055.

[30]Srinivasan, S. G., Van Duin, A. C., and Ganesh, P., "Development of a ReaxFF potential for carbon condensed phases and its application to the thermal fragmentation of a large fullerene," *The Journal of Physical Chemistry A*, Vol. 119, No. 4, 2015, pp. 571–580.

[31]de Tomas, C., Suarez-Martinez, I., and Marks, N. A., "Graphitization of amorphous carbons: A comparative study of interatomic potentials," *Carbon*, Vol. 109, 2016, pp. 681–693.

[32]Poovathingal, S., Schwartzentruber, T. E., Srinivasan, S. G., and Van Duin, A. C., "Large scale computational chemistry modeling of the oxidation of highly oriented pyrolytic graphite," *The Journal of Physical Chemistry A*, Vol. 117, No. 13, 2013, pp. 2692–2703.

[33]Hahn, J., "Kinetic study of graphite oxidation along two lattice directions," *Carbon*, Vol. 43, No. 7, 2005, pp. 1506–1511.

[34]Klemens, P. and Pedraza, D., "Thermal conductivity of graphite in the basal plane," *Carbon*, Vol. 32, No. 4, 1994, pp. 735–741.

[35]Nika, D., Ghosh, S., Pokatilov, E., and Balandin, A., "Lattice thermal conductivity of graphene flakes: Comparison with bulk graphite," *Applied Physics Letters*, Vol. 94, No. 20, 2009, pp. 203103.

[36]Alofi, A. and Srivastava, G., "Thermal conductivity of graphene and graphite," *Physical Review B*, Vol. 87, No. 11, 2013, pp. 115421.

[37]Zhu, T., Swaminathan-Gopalan, K., Cruse, K. J., Stephani, K., and Ertekin, E., "Vibrational energy transport in hybrid ordered/disordered nanocomposites: Hybridization and avoided crossings of localized and delocalized modes," *Advanced Functional Materials*, Vol. 28, No. 17, 2018, pp. 1706268.

[38]Zhu, T., Swaminathan-Gopalan, K., Stephani, K., and Ertekin, E., "Thermoelectric phonon-glass electron-crystal via ion beam patterning of silicon," *Physical Review B*, Vol. 97, No. 17, 2018, pp. 174201.

[39]Swaminathan-Gopalan, K., Zhu, T., Ertekin, E., and Stephani, K. A., "Structural and thermal effects of ion-irradiation induced defect configurations in silicon," *Physical Review B*, Vol. 95, No. 18, 2017, pp. 184109.